Modeling and analysis of the influence caused by micro-vibration on satellite attitude control system

Lin Li [a,b,e,1], Yang Yu [c,d,f,1], Li Wang [a,b], Li Yuan [a,b,e,*], Lei Zhang [c,d,f], Xiaoxue Gong [f], Yanpeng Wu [a,b], Ran Zheng [a,b]

[a] Space Optoelectronic Measurement and Perception Lab., Beijing Institute of Control Engineering, Beijing, 100190, China
[b] China Academy of Space Technology, Beijing, 100094, China
[c] University of Chinese Academy of Sciences, Beijing, 100049, China
[d] Changchun Institute of Optics, Fine Mechanics and Physics, Chinese Academy of Sciences, Changchun, 130033, China
[e] National Key Laboratory of Space Intelligent Control , Beijing, 100094, China
[f] Chang Guang Satellite Technology Co., Ltd., Changchun, 130102, China

ARTICLE INFO

ABSTRACT

A closed-loop integrated model including micro-vibration disturbance, dynamic characteristics of satellite, optical system of star sensor and attitude control algorithm is established. The control torque error caused by additional disturbance torque and the star sensor imaging error caused by structural resonance is fully integrated analyzed, which are firstly presented into the attitude control system (ACS). Steady-state and transient response analyses are completed to evaluate the impact of such two errors on performances of (ACS). Steady-state response results show that the effect of control torque error appears in lower frequency band with a peak of 6.784E-8″ at 53 Hz, while influence of star sensor imaging error on attitude determination mainly concentrates in high frequency band with maximum response of 0.4101″ at 315 Hz. Transient response results show that the two errors will not significantly affect control indicators such as rise time, overshoot and peak time. The results indicate that the influence of star sensor imaging error is non-negligible for satellite ACS which required milli-arc-second attitude control accuracy. According to the analytical results, traditional analysis only on payload optical axis cannot reveal the whole impact of micro vibration on LOS error, the two errors of micro-vibration introduced to ACS in this work must be considered for the development of spacecraft with 0.1″ pointing accuracy.

1. Introduction

With the development of spacecraft remote sensing performance and the versatility of functions, there exists an increasing requirement on ultra-precise pointing measurement and attitude control for current and future space systems [1–3]. The pointing measurement accuracy of earth observation satellites has reached angular second accuracy [4–8]. As for deep space probes, higher attitude control accuracy is usually required [1,9,10]. Such as, the angular resolution of Hubble Space Telescope is 0.1″, and the pointing accuracy of James Webb Space Telescope is expected to reach four milli-arc-seconds [4].

As the actuator of spacecraft's attitude control system (ACS), flywheel is indispensable. Due to very tiny manufacture errors and defects, micro-vibration will be produced with small amplitude and wide

frequency bandwidth [1,11,12]. At present, large numbers of studies have deeply analyzed the influence of micro-vibration on spacecraft payload's line-of-sight (LOS). The micro-vibration disturbance, and transfer function have been discussed by integrating structural and the optical payload system, thus the effect of the micro-vibration on payload LOS can be output accurately. Furthermore, a large number of ground or in-orbit tests have proved the accuracy of these studies [3,13–20]. However, most of these studies focus on the impact of micro vibration on the service level of optical payload [13,15,17–20], and the ACS offset caused by control torque error and star sensor imaging error induced by micro-vibration has not attracted serious attention.

In previous studies, we presented an integrated model to estimate the impacts of micro-vibration on optical payload [21], the image motion of a 0.1″ space pointing measuring instrument for micro-vibration
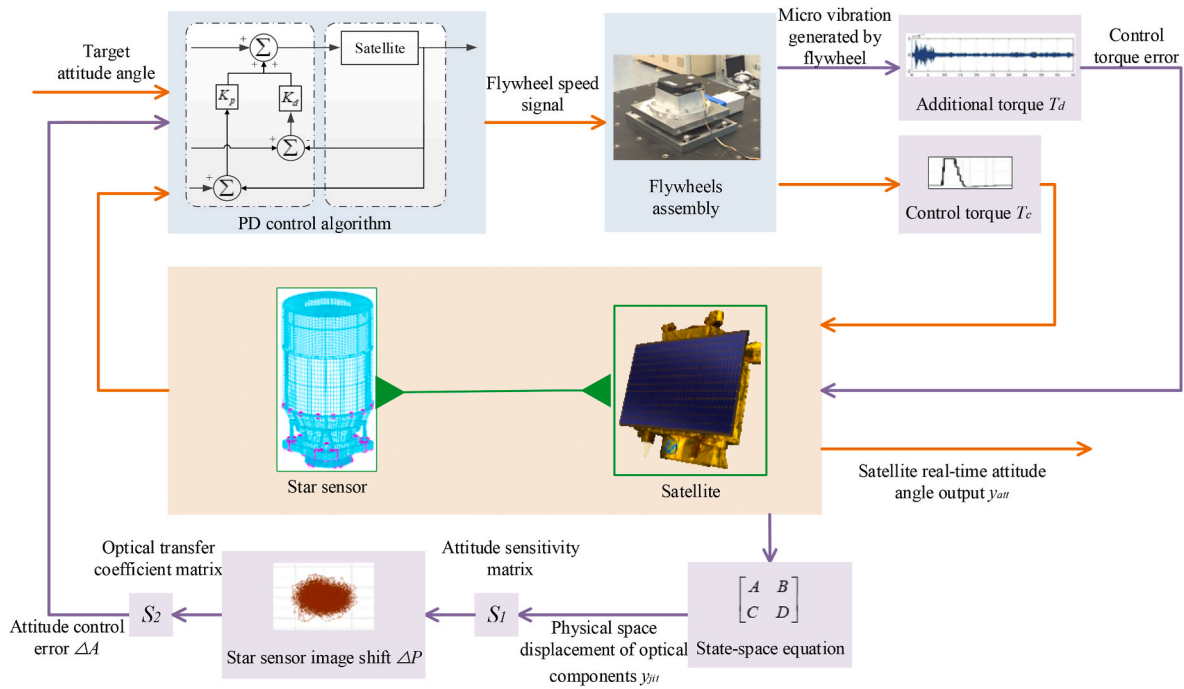

Fig. 1. Schematic diagram of the overall closed-loop framework.

conditions were experimentally studied [10], and the random measurement errors of the micro-vibration test platform caused by electronic and mechanical noises were discussed in depth [22]. However, micro-vibration produces two errors in ACS, which may reduce the accuracy of ACS. One is control torque error, and the other is star sensor imaging error. Firstly, the flywheel provides control torque for the spacecraft to maneuver its attitude. Additional torques cause deviations between actual and theoretical control torques, resulting in errors in the course of attitude translation [11,12]. Secondly, Star sensor obtains real-time attitude information by imaging stars and analyzing their relative positions. Hence, when the optical components in star sensor resonate with micro-vibration, the imaging will deviate, resulting in attitude calculation errors [1,3,10,12,and14]]. The attitude errors feedback to control algorithm will lead to the inaccuracy of attitude determination.

This paper makes a depth study on the influence mechanism of control torque error and star sensor imaging error induced by micro-vibration on ACS. An integrated model including micro-vibration disturbance, dynamic characteristics of platform structure, optical system of star sensor and attitude control algorithm is established. Therefore, the control torque error and the star sensor imaging error are firstly presented into the integrated model, and the influences of ACS are thoroughly analyzed. Transient response results show that the two errors will not significantly affect control indicators. Steady-state response results show that the effect of control torque error appears in lower frequency band with small magnitude, and the influence of star sensor imaging error mainly concentrates in high frequency band with considerable magnitude.

The content of work is divided into five parts. In Section 2, an integrated modeling method and the two error models are established. In Section 3, the extraction method of parameters in integrated model is introduced based on a spacecraft principal prototype. In Section 4, the results of transient and steady-state response are presented, and the influence mechanism of the two errors on ACS is analyzed respectively. Section 5 is the conclusion part of this paper.

2. ACS micro-vibration integrated modeling

ACS is responsible for attitude maneuver when spacecraft changes its working modes [23,24]. A typical ACS flow chart mainly includes four parts, that is, control algorithm subpart, flywheel assembly subpart, star sensor subpart and satellite structure subpart. The control algorithm subpart is responsible for generating speed signal according to the target attitude angle for flywheel assembly. The flywheel assembly subpart is responsible for outputting control torque that acts on spacecraft, in which the optical payload and star sensor are both assembled. The star sensor subpart is responsible for obtaining real-time attitude angle information and feedback it into control algorithm. The satellite structure subpart is responsible for transmitting the disturbance torque and control torque from flywheel assembly to star sensor. Above subparts can be integrated into a closed-loop model in state-space equation form, in which the control algorithm applies Proportional-Derivative (PD) controller, the flywheel disturbance input is calculated by harmonic superposition, and the star sensor and satellite are described in the form of state-space equation. A typical ACS dynamic equation is expressed in state-space as Equation (1) given below [12].

$$
\begin{bmatrix} \dot{\eta} \\ \dot{x}_c \\ y_{att} \end{bmatrix} = \begin{bmatrix} A + B_{T_c}D_cC_{att} & B_{T_c}C_c & B_{T_c}D_cD_{T_c\_att} \\ B_cC_{att} & A_c & B_cD_{T_c\_att} \\ C_{att} & C_cD_{T_c\_att} & D_cD_{T_c\_att} \end{bmatrix} \begin{bmatrix} \eta \\ x_c \\ T_c \end{bmatrix} \tag{1}
$$

where, η is state vector representing the coordinates in modal space, T_c is input vector representing control torque y_{att} is output vector representing the information of attitude angle, x_c represents the attitude observation channel, the significance of observation channel is to observe the attitude information of spacecraft at all times and feed attitude information back to ACS so as to adjust the attitude of the spacecraft at all times. A, B_{T_c}, C_{att} and $D_{T_c\_att}$ are structural dynamics parameters of spacecraft, which are determined by Equation (2), A_c, B_c, C_c and D_c are ACS parameters, which are determined by Equation (3). The change of attitude angle y_{att} of spacecraft caused by control torque T_c can be obtained by Equation (2). ACS can calculate the control torque T_c required for the next moment according to attitude angle y_{att} through Equation (3). This paper assumes that the nonlinearity of prototype structure can be neglected. Modal superposition method is usually used

to solve the mechanical responses of such linear complex structure. According to this method, each mode (or eigenvector) that participates in calculation is linearly independent. Therefore, the state-space equation of the modal superposition method can be written in linear form as shown in Equation (2) [25–27].

$$\begin{bmatrix} \dot{\eta} \\ y_{att} \end{bmatrix} = \begin{bmatrix} A & B_{T_c} \\ C_{att} & D_{T_c\_att} \end{bmatrix} \begin{bmatrix} \eta \\ T_c \end{bmatrix} \tag{2}$$

$$\begin{bmatrix} \dot{x}_c \\ T_c \end{bmatrix} = \begin{bmatrix} A_c & B_c \\ C_c & D_c \end{bmatrix} \begin{bmatrix} x_c \\ y_{att} \end{bmatrix} \tag{3}$$

Traditional ACS can be represented by the above equation, and the orange line in Fig. 1 is more intuitive. The parameters in ACS system can be directly expressed as observation channels by state-space, and the state matrix can be directly established by structural parameters of spacecraft itself, which simplifies the modeling process and it retains the dynamic characteristics of the spacecraft.

With the increasing requirement of attitude control accuracy for spacecraft, the error of ACS component is no negligible. Therefore, the influence of micro-vibration on ACS needs to be studied in depth. The reason for the influence of star sensor imaging error is that star sensor is an optical system, when it is affected by micro-vibration, internal optical components will be unstable, resulting in the error of obtaining attitude information, the error of attitude information fed back to control algorithm will cause inaccurate attitude determination. Control torque error is an ineradicable error between the actual control torque and the theoretical control torque, accounted by the manufacture error of flywheel, it affects the accuracy of attitude determination at non-negligible degree. Based on the traditional ACS model, this paper integrated two error models colored purple in Fig. 1.

According to the physical models of the two errors in Fig. 1, the two error models can be introduced into the traditional integrated model. Equation (4) is the state-space model considering control torque T_d and micro-vibration response output y_{jit}. Equation (5) is the state-space model considering star sensor image error ΔA. Equation (6) is the global ACS model.

$$\begin{bmatrix} \dot{\eta} \\ y_{att} \\ y_{jit} \end{bmatrix} = \begin{bmatrix} A & B_{T_c} & B_{T_d} \\ C_{att} & D_{T_c\_att} & D_{T_d\_att} \\ C_{jtt} & D_{T_c\_jit} & D_{T_d\_jit} \end{bmatrix} \begin{bmatrix} \eta \\ T_c \\ T_d \end{bmatrix} \tag{4}$$

$$\begin{bmatrix} \dot{x}_c \\ T_c \end{bmatrix} = \begin{bmatrix} A_c & B_c \\ C_c & D_c \end{bmatrix} \begin{bmatrix} x_c \\ y_{att} + \Delta A \end{bmatrix} \tag{5}$$

$$\begin{bmatrix} \dot{\eta} \\ \dot{x}_c \\ y_{att} \end{bmatrix} = \begin{bmatrix} A + B_{T_c}D_cC_{att} & B_{T_c}C_c & B_{T_d} + B_{T_c}D_cD_{T_d\_att} \\ B_cC_{att} & A_c & B_cD_{T_d\_att} \\ C_{jit} + D_{T_c\_jit}D_cC_{att} & D_{T_c\_att}C_c & D_{T_d\_jit} + D_{T_c\_jit}D_cD_{T_d\_att} \end{bmatrix} \begin{bmatrix} \eta \\ x_c \\ T_c \end{bmatrix} \tag{6}$$

2.1. Modeling of control torque error

Micro-vibration disturbances of flywheel is the primary factor that produce control torque error, they are made up of structural modal disturbances and harmonic disturbances [12]. Modal disturbances are related to the installation flexibility of flywheel whose frequencies can be adjusted out of sensitive frequency band through reasonable-design, and influences are avoidable through proper installation structure design. However, influences of harmonic disturbance are hard to avoid due to their broadband characteristics. According to previous researches [12], harmonic disturbances are generated by static imbalance, dynamic imbalance of rotor and defects of bears assembled in flywheel, performing unwanted forces and torques whose magnitudes are linear with the square of wheel speeds, as shown in Equation (7):

$$X_j(t) = \sum_{i=1}^{n} A'_{ij}\Omega^2 \cos\left(h_{ij}\Omega t + p'_{ij}\right) \tag{7}$$

where, $X_j(t)$ represents disturbance in one direction, A'_{ij} and p'_{ij} are respectively harmonic amplitude coefficient and harmonic initial phase of each disturbance force or disturbance torque, and h_{ij} represents corresponding harmonic factor, Ω represents the speed of flywheel.

Equation (7) is processed by Fast Fourier Transform to obtain Equation (8) [11].

$$X_j(\omega) = \sum_{i=1}^{n} \pi A'_{ij}\Omega^2 \left(\cos p'_{ij} + j\sin p'_{ij}\right)\delta(\omega - h_{ij}\Omega) \tag{8}$$

It can be seen from Equation (8) that the peak occurs at $\omega = h_{ij}\Omega$, and the peak value is proportional to the square of flywheel speed. Typical disturbance peak appears on a series of harmonic lines whose frequency is proportional to flywheel speed. When the speed of flywheel is Ω, the micro-vibration disturbance of a single flywheel in time-domain can be obtained as Equation (9).

$$T_d(t) = \sum_{i=1}^{n} A_{ij}(t)\Omega^2 \cos\left[h_{ij}\Omega(t)\tau_t(t) + p_{ij}(t)\right] \tag{9}$$

where A_{ij} and p_{ij} are respectively the amplitude and initial phase of each order harmonic obtained by interpolating the harmonic characteristics through the test data, and τ_t represents simulation time.

2.2. Modeling of star sensor imaging error

The dynamic differential equation of satellite can be described by Equation (10) [21].

$$M\ddot{x} + C\dot{x} + Kx = T_d + T_c \tag{10}$$

where M, C and K represents mass matrix, damping matrix, and stiffness matrix respectively, x represents nodes displacement in physical space.

The solar array of spacecraft studied in this paper is rigidly connected to the spacecraft, and its installation rigidity is about 100 Hz and the control bandwidth of the ACS is only 4 Hz. Therefore, the flexibility of the solar array will not significantly affect ACS. Based on the finite element model (FEM) and using the modal superposition method, Equation (10) is transformed from physical space to modal space form, which is shown as Equation (11), through multiplying both sides of the equation by mass-normalized mode shape matrix.

$$\ddot{q} + 2\varepsilon\omega\dot{q} + \omega^2 q = \varphi^T(T_d + T_c) \tag{11}$$

where q represents modal coordinate, the first r-order mode (ignore rigid body modes) are selected, $q \in R^{r\times 1}$, ε and ω represents diagonal modal damping matrix and diagonal frequency matrix, φ^T represents mass-normalized mode shape matrix.

Equation (4) is the form described in state-space equation of equation (11). The system matrix expression is:

$$\begin{bmatrix} A & B_{T_d} & B_{T_c} \\ C_{att} & D_{T_d\_att} & D_{T_c\_att} \\ C_{jtt} & D_{T_d\_jit} & D_{T_c\_jit} \end{bmatrix} = \begin{bmatrix} -\omega^2 & -2\varepsilon\omega & \varphi^T\alpha_{T_d} & \varphi^T\alpha_{T_c} \\ 0 & I & 0 & 0 \\ 0 & \varphi\beta_{T_d} & 0 & 0 \\ 0 & \varphi\beta_{T_c} & 0 & 0 \end{bmatrix} \tag{12}$$

where α and β are modal selection matrices. The function of α is to input micro-vibration disturbance, input T_d and control input T_c from the position of flywheel, while the function of β is to locate output position at concerned nodes such as the mirrors inside star sensor.

To obtain the modal information ε, ω and φ^T in Equation (12), the finite element model (FEM) is built in finite element software following the principles given below:
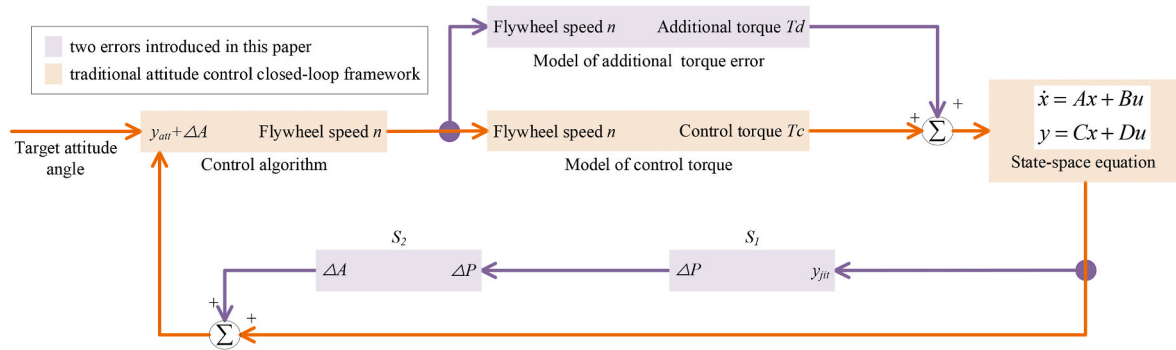
(1) Flywheel is approximated as a mass node.

Fig. 2. Integrated models built in numerical calculation framework.

(2) Take the unconstrained structural modes within frequency band of interest (0–500 Hz in this paper).

(3) FEM has no boundary constraint and no applied load.

(4) In FEM, most of structures are hexahedral elements, and thin-walled structures are quadrilateral elements.

With the modal superposition method and the state space transfer function, the response output y_{jit} of each mirror in the physical space can be obtained by Equation (4). After obtaining micro-vibration response output y_{jit}, an optical system model is required to convert y_{jit} to an optical index (image motion ΔP).

Since the perturbation of the micro-vibration is very small, the displacement of optical components is also very small. Based on the paraxial optics theory in geometric optics, the physical space displacement response of components can be mapped to the image motion response. The acquisition process of optical system parameters is described in-detail in Section 3.3

$$\Delta P = S_1 y_{jit} \tag{13}$$

where $S_1 \in R^{2 \times n_{mi}}$ represents optical transfer coefficient matrix, which can be obtained through optical calculation, n_{mi} represents the number of optical components. $\Delta P = \begin{bmatrix} \Delta x & \Delta y \end{bmatrix}^T$ represents the image motion of the star sensor in two directions.

2.3. Pointing error analysis

Control torque error and star sensor imaging error caused by micro-vibration can be converted into image motion by above modeling method. The offset of the LOS of star sensor ΔL can be obtained by Equation (14).

$$\Delta L = \Delta P / f \tag{14}$$

where f represents the focal length of star sensor. This offset is equivalent to the measurement error of star sensor. According to the installation position of star sensor on spacecraft and according to Equation (15), the pointing error of the spacecraft can be obtained.

$$\Delta A = \begin{bmatrix} s_{ij}^n \end{bmatrix} \Delta L = \begin{bmatrix} s_{ij}^n \end{bmatrix} \Delta P \Big/ f = S_2 \Delta P \tag{15}$$

where s_{ij}^n represents the coefficient from the i direction of the number-n star sensor to the j direction of spacecraft. Attitude determination error is linearly added to the measurement result of star sensor which under normal conditions, and then it can be integrated into the overall closed-loop framework.
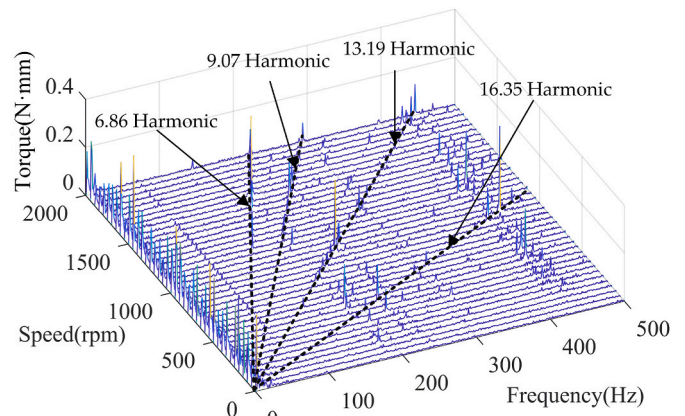

Fig. 3. Campbell diagram of disturbance torque My.

Table 1
The number of harmonics.

Flywheels	X-flywheel	Y-flywheel	Z-flywheel
Fx	157	159	120
Fy	177	174	128
Fz	90	90	52
Mx	173	207	113
My	150	181	111

3. Semi-physical simulation

3.1. Integration simulation architecture

In Fig. 2, the orange parts are the traditional ACS model, in which the parameters are based on a Spacecraft and input its real ACS parameters into the model. At present, researchers have made more in-depth study on the traditional ACS model, which is not the focus of this paper. The purple part represents two errors introduced in this paper, and its specific parameters will be described in detail below.

3.2. Parameters of control torque error

The parameters of control torque error are calculated from test data that is obtained from 'Kistler' measurement system [12]. Fig. 3 shows an example of the processed test data in form of Campbell diagram.

Harmonic characteristics are quite obvious as shown in Fig. 3. In this figure, 4 typical harmonics are extra marked. However, there are actually hundreds of harmonics which are unobservable via eyes in this figure. To capture these harmonics, this paper develops a harmonic identify algorithm. Through linearity identification of frequencies of

Table 2
Key parameters of peak typical harmonics.

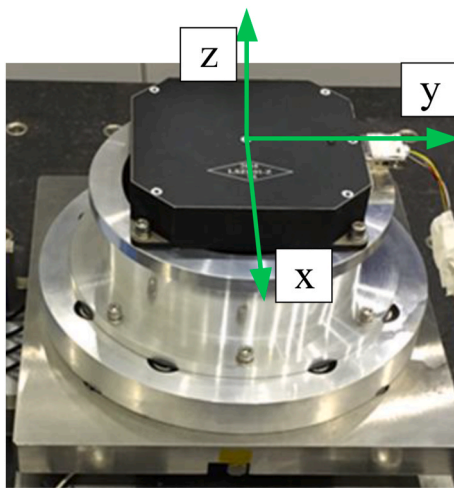| Flywheels	Disturbance	A_{ij} (N/RPM^2 or N·m/RPM^2)	h_{ij} (60*Hz/RPM)	p_{ij} (rad)
X-flywheel	Fx	2.697E-06	9.214	−0.064
	Fy	2.702E-06	8.808	−0.342
	Fz	2.390E-06	10.07	0.919
	Mx	1.654E-07	3.046	1.316
	My	1.561E-07	6.740	1.600
Y-flywheel	Fx	1.812E-06	8.721	−1.407
	Fy	3.351E-06	9.314	1.129
	Fz	4.383E-06	12.58	0.975
	Mx	3.726E-07	1.54	−2.120
	My	2.056E-07	3.012	−2.394
Z-flywheel	Fx	1.937E-06	9.003	−0.010
	Fy	1.144E-06	8.994	2.889
	Fz	1.704E-06	10.49	−1.003
	Mx	1.449E-07	3.674	0.536
	My	2.364E-07	6.826	−1.735

Table 3
Dimensions of the state matrix and the state vector.

Nomenclature	State vector	Dimensions
State matrix	A	$A \in R^{252 \times 252}$
	A_c	$A_c \in R^{6 \times 6}$
	B_{T_c}	$B_{T_c} \in R^{252 \times 6}$
	B_{T_d}	$B_{T_d} \in R^{252 \times 6}$
	B_c	$B_c \in R^{6 \times 6}$
	C_{att}	$C_{att} \in R^{252 \times 6}$
	C_{jit}	$C_{jit} \in R^{6 \times 252}$
	C_c	$C_c \in R^{6 \times 6}$
	$D_{T_c\_att}$	$D_{T_c\_att} \in R^{6 \times 6}$
	$D_{T_c\_jit}$	$D_{T_c\_jit} \in R^{6 \times 6}$
	$D_{T_d\_att}$	$D_{T_d\_att} \in R^{6 \times 6}$
	$D_{T_d\_jit}$	$D_{T_d\_jit} \in R^{6 \times 6}$
	D_c	$D_c \in R^{6 \times 6}$
State vector	η	$\eta \in R^{252 \times 1}$
	x_c	$x_c \in R^{6 \times 1}$
	x_c	$x_c \in R^{6 \times 1}$
	T_c	$T_c \in R^{6 \times 1}$
	y_{att}	$y_{att} \in R^{6 \times 1}$

Fig. 4. Frame definitions of disturbing forces and torques.
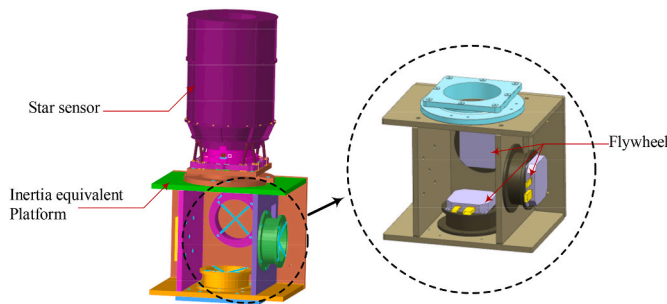
Fig. 5. The FEM of the system principal prototype.

Table 4
The calculation results of S_1

Attitude determination error	Mirror	Displacement of mirrors (1 mm)		Rotation of mirrors (1°)	
		X	Y	X	Y
U-direction (mm)	Mirror 1	−1.05E-1	0	0	4.67
	Mirror 2	−2.92E-1	0	0	7.50E-2
	Mirror 3	−2.92E-1	0	0	−1.20E-2
	Mirror 4	4.25E-1	0	0	4.36E-2
	Mirror 5	1.26	0	0	−1.07E-2
V-direction (mm)	Mirror 1	0	−1.05E-1	−4.67	0
	Mirror 2	0	−2.92E-1	−7.50E-2	0
	Mirror 3	0	−2.92E-1	1.20E-2	0
	Mirror 4	0	4.25E-1	−4.36E-2	0
	Mirror 5	0	1.26	1.07E-2	0

3.3. Star sensor imaging error model

The study object in this paper is a satellite principal prototype of which the FEM is shown in Fig. 5. The moment of inertia of the spacecraft is [1.00 2.49 2.41] kg·mm, the maximum torque of flywheel is 2 N·m. This FEM model has 126 order modes in the range of 500 Hz. Therefore, the dimensions of the state matrix and the state vector in Equation (6) are shown in Table 3. Lanczos method based on vector superposition is used for kinetic analysis. This paper analyzes the modes in the range of 0–500hz, and the modal damping used in this work is 0.003 [12,28]. Dimensions of state vectors in state space Equation (1) and Equation (2) are related to mode order and degree-of-freedom (see Table 4).

The FEM of flywheel is approximated as a mass point. Through modal selection matrix α, additional torque input T_d and control input T_c are applied on flywheel mass point. By Adjusting modal selection matrix , the input position of micro-vibration source and control torque at flywheel can be located. The response of optical system components inside star sensor is set as the output of FEM kinetic model.

The optical system of star sensor is mainly composed of five mirrors
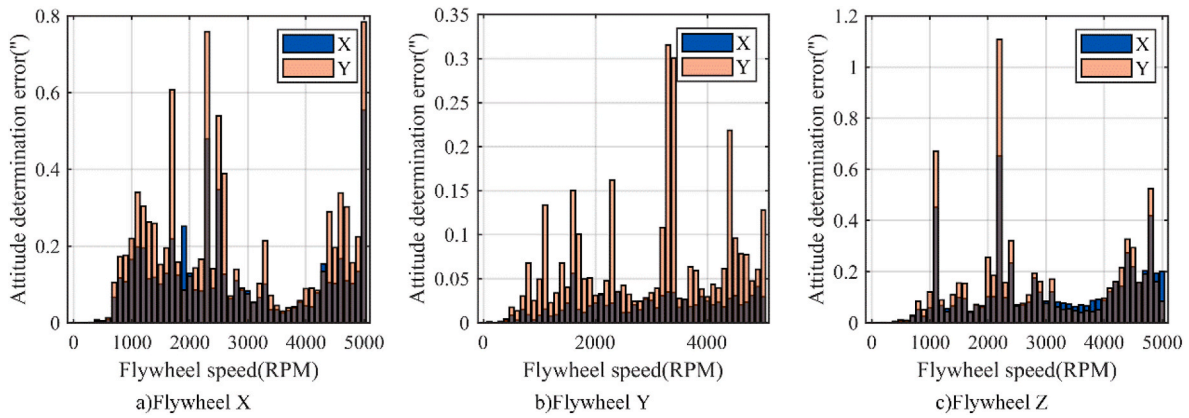
data whose magnitudes are twenty times higher than background noises, harmonics are identified from vast test data. Through least square method, h_{ij}, A_{ij} and p_{ij} are obtained for each harmonic located in speed range of 0 RPM to 5000 RPM and frequency range of 0 Hz–500 Hz. Table 1 summaries these harmonical disturbances in all directions of each test flywheel while Table 2 shows several representative harmonics in each direction with their corresponding key parameters. The fame of Fx, Fy, Fz, Mx, and My in Table 2 is defined on a single flywheel in Fig. 4, wherein the z axis coincides with the spin axis of the flywheel, y axis coincides with the electrical interface, and x axis is defined following the Right-Hand Rule, and the definition of 'X, Y and Z-flywheel' is base one the frame of satellite principal prototype.

Fig. 6. Maximum attitude determination error caused by micro-vibration.

Table 5
Statistics of maximum attitude determination error.

Flywheels	Deviation value (″)	Speed (RPM)	Direction
X-flywheel	0.6071	1700	Y
	0.7587	2300	Y
	0.5390	2500	Y
	0.7837	5000	Y
Y- flywheel	0.3154	3300	Y
	0.3005	3400	Y
Z- flywheel	0.6703	1100	Y
	1.1070	2200	Y
	0.5249	4800	Y
	0.6513	2200	X

and a focal plane. For this optical system, micro-vibration affects imaging mainly due to the micro-vibration response of five mirrors and focal plane. Optical transfer coefficient matrix S_1 and attitude sensitivity matrix S_2 of the six optical components can be obtained through optical computing software.

Micro-vibration may cause the optical components to jitter and deviate from the initial position. When any optical component changes in position, it will cause image motion on focus plane. In the case of small disturbance, it can be regarded as a Taylor expansion of the optical path length of a uniformly incident beam through the optical system [19]. Since the magnitude of micro-vibration disturbance is very small, higher-order terms can be ignored. Image point movement on focal plane can be resolved into the displacement and rotation functions of the various optical components.

$$\Delta P = S_1 y_{jit} = \sum_{i=1}^{N} \partial L/\partial T_i \cdot \Delta T_i + \sum_{i=1}^{N} \partial L/\partial R_i \cdot \Delta R_i \quad (16)$$

where ΔT_i and ΔR_i represent displacement and rotation vectors of each optical components, $\partial L/\partial T_i$ and $\partial L/\partial R_i$ represent displacement and rotation transfer coefficients. The displacement of optical components caused by micro-vibration can be transformed into the image motion ΔP by Equation (16), and then the attitude determination error ΔA can be obtained. Table 5 shows the calculation results of S_1. Taking the data "-1.05E-1″" as an example, it shows that when the Mirror 1 has a 1 mm displacement on X-direction, the attitude determination will have an error of $-1.05\text{E-}1$ mm on U-direction. U-direction and V-direction are two components in the focal plane perpendicular to the LOS.

4. Results and discussion

There are two working stages for the ACS in orbit; they are stabilization stage and maneuver stage. In stabilization stage, the payload of the satellite begins to work. In addition, the main purpose of ACS is to maintain the stability of LOS. In maneuver stage, satellites rotate from initial attitude angle to target attitude angle according to the command. This process generally requires small rise time, low overshoot and short peak time. By analyzing the steady-state parameters of the stabilization
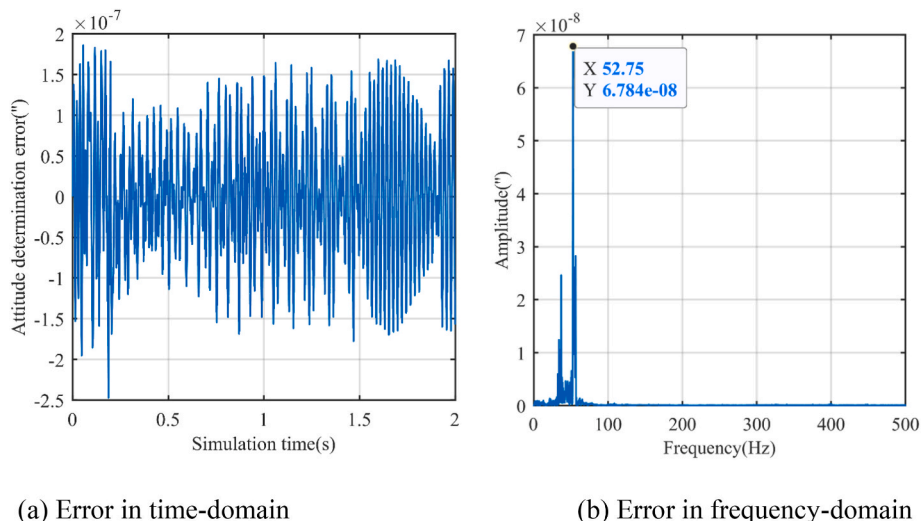

(a) Error in time-domain

(b) Error in frequency-domain

Fig. 7. Attitude determination error caused by control torque error.

(a) Error in time-domain   (b) error in frequency-domain
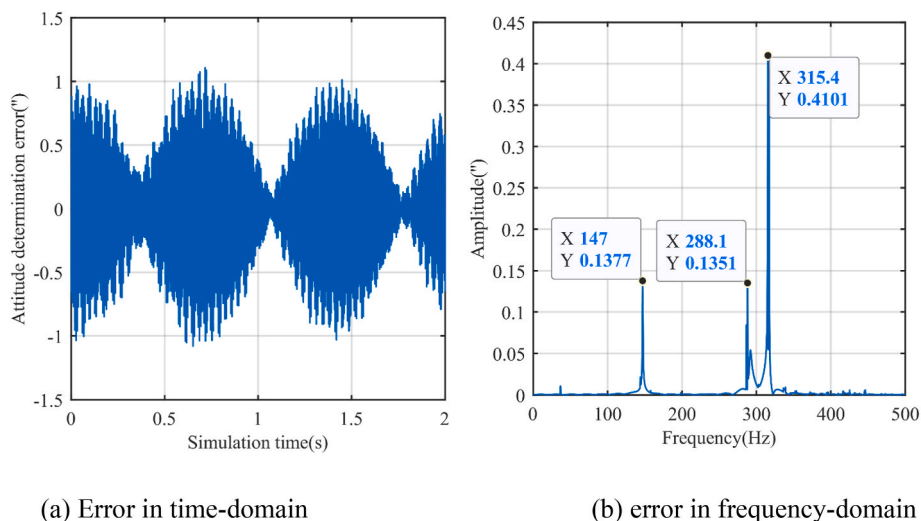
Fig. 8. Attitude determination error caused by star sensor imaging error.

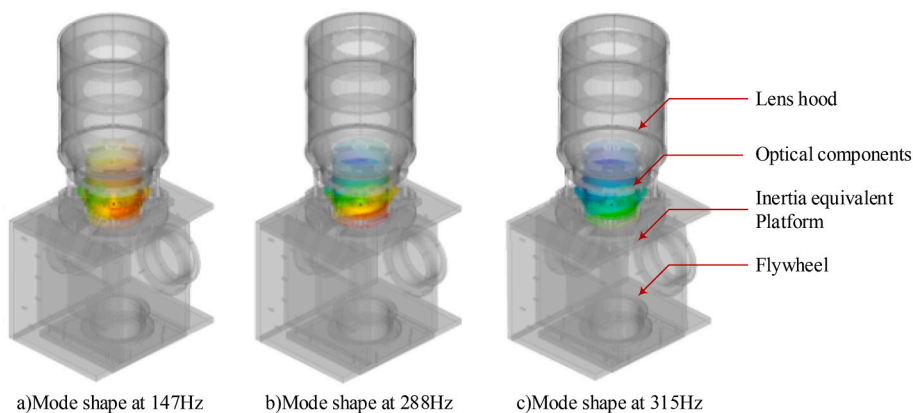a)Mode shape at 147Hz   b)Mode shape at 288Hz   c)Mode shape at 315Hz

Fig. 9. Schematic diagram of mode shape.

stage and the transient parameters of the maneuver stage, this paper deeply studies the influence of micro-vibration on ACS.

4.1. Stabilization state response results

Fig. 6 and Table 5 shows the maximum attitude determination error caused by micro-vibration at stabilization sets when one flywheel works independently with the other two flywheels do not rotate. The maximum deviation which reaches 1.107″ at 2200 RPM is produced by flywheel-Z around Y-axis of satellite. In order to deeply study the cause of the deviation, this paper analyzes and studies the situation that the two errors are introduced separately at this speed.

Fig. 7(a) shows the attitude determination error caused by control torque error in time-domain at the speed of 2200RPM. Fig. 7 (b) gives the response of satellite attitude determination error in frequency-domain. It can be seen from Fig. 7 (a) that the magnitude of attitude determination error is 10e-7. Compared with the error of 1.107″, the proportion is very small. In Fig. 7 (b), a peak appears in frequency-domain results at 53 Hz. Since there is no structural mode closed to this frequency according to the modal analysis of the principal proto-type, the reason for this response is not resonance, but the excitation of the first harmonic of micro-vibration, with an amplitude of 6.784e-8″. It can be concluded that the control torque error can be ignored when analyzing the influence of micro-vibration on ACS.

In Fig. 8 (a), the maximum attitude determination error reaches to 1″. Compared with control torque error, star sensor imaging error

becomes the more critical reason influencing the attitude determination of ACS. In Fig. 8 (b), three peaks appear at 147 Hz, 288 Hz and 315 Hz respectively. Through finite element analysis, it can be obtained that there are structural modes at these three frequencies that are shown in Fig. 9. The peak of Fz-disturbance caused by flywheel-Z is at 314 Hz. Therefore, at 314 Hz, the micro-vibration disturbance of the flywheel will excite the structural mode of star sensor and resonance is produced. There are also disturbing frequencies closed to 147 Hz and 288 Hz (152 Hz and 283 Hz respectively), and the disturbing amplitude at these two frequencies are smaller than that at 314 Hz. Hence, resonances also appear at 147 Hz and 288 Hz with smaller peaks. Compared with control torque error, the influence of star sensor imaging error on attitude determination accuracy is enormous. Star sensor imaging error is the main reason for the influence of micro-vibration on attitude determination.

4.2. Maneuver stage response

The integrated modeling method proposed in this work can predict the influence of flywheel micro-vibration on satellite attitude control links under various maneuver conditions. The change of satellite attitude on-orbit is complex, and it will change to a target attitude angle with different initial attitude angle and different initial attitude angular velocity. Since it is impossible to analyze all maneuver conditions, this paper selects three basic maneuver conditions with different initial attitude angle, target attitude angle, initial flywheel speed and initial

Table 6
Simulation related parameters.

Parameters	maneuver condition 1	maneuver condition 2	maneuver condition 3
Initial attitude angle	[2,7,8] °	[0,3,5] °	[1,2,5] °
Target attitude angle	[3,5,6] °	[1,2,4] °	[3,7,8] °
Initial flywheel speed	[1500,2500,3500] RPM	[100,200,300] RPM	[500,500,500] RPM
Initial attitude angular velocity of satellite	[0.1,0.2,0.3] °/s	[0.0,0.0,0.0] °/s	[-0.2, −0.1,0.3] °/s

attitude angular velocity of satellite, which can comprehensively cover a variety of maneuver conditions. Three maneuver condition sets are given as examples in Table 6.

Figs. 10–12 are three-axis attitude angle change curves under three maneuver conditions. In each figure, they are a) without any interference b) introducing star sensor imaging error and c) introducing additional torque. Table 7 shows the statistics of transient parameters. The ACS of most satellites is designed with critical damping or over damping, which is to reduce the vibration of the satellite in the maneuver stage and consequently to protect the structure of the satellite from damage. In this work, PD control strategy and over-damping mode are adopted so that overshoot and peak time will not be important factors affecting ACS performance. As for the rise time it can be concluded from Table 6 that after introducing the two errors, the maximum rise time changes no more than 0.001s, therefore, the micro-vibration will not significantly affect the maneuver stage.

4.3. Discussion

Ultra-performance spacecraft usually refers to Ultra-Accuracy Ultra-Stability Ultra-Agility, and the precision pointing performance (~milli-arc-sec) is the primary requirement. In orbit flying spacecraft, there will be a lot of interference. For example, aerodynamics, micro meteor impact force, uneven gravity caused by the oblations of the earth and solar radiation pressure. In addition, the internal motion mechanism of spacecraft, such as flywheel assemblies [1,3,8,12], will also produce interference force. Although this interference forces are very small, the air in space is thin enough to change the fine pointing of spacecraft [1,3, 29]. These low-level mechanical vibration or disturbance in space environment, typically occurring at frequency from less than 1 Hz up to a few kHz [12,30]. Due to very tiny environmental damping (~1/25 of the ground) in aerospace, micro-vibration could persist for a very long time. This will deteriorate the working environment of the ACS. This phenomenon is further proved by the method in this work.

The analysis results in this work show that micro vibration of flywheel will cause an error of about one-arc-second on ACS. This proves that it is not enough to analyze the influence of micro vibration on LOS; the errors of star sensor caused by micro vibration should be introduced into the full-closed-loop simulation model. At present, most star sensors and satellite platform are rigidly connected, which provides a good path for the transmission of micro vibration. This may cause resonance of opto-mechanical structure of star sensor, and then affect the attitude process. Therefore, for ultra-performance spacecraft it is very necessary to adopt vibration isolation design for flywheel or/and star sensors.

There exists an increasing need for milli-arc-seconds accuracy pointing measurement for current and future space systems, and the
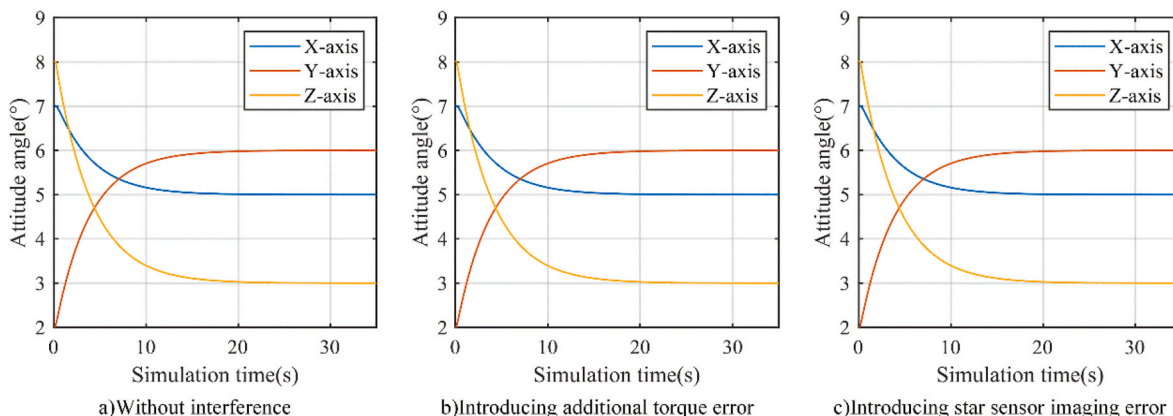

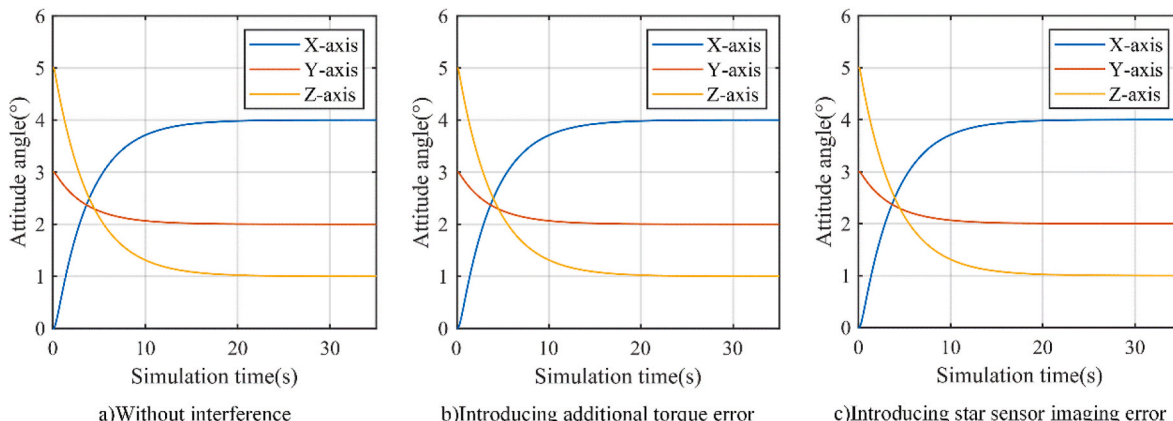**Fig. 10.** Attitude angle change curve of maneuver condition #1.

Fig. 11. Attitude angle change curve of maneuver condition #2.

a)Without interference   b)Introducing additional torque error   c)Introducing star sensor imaging error
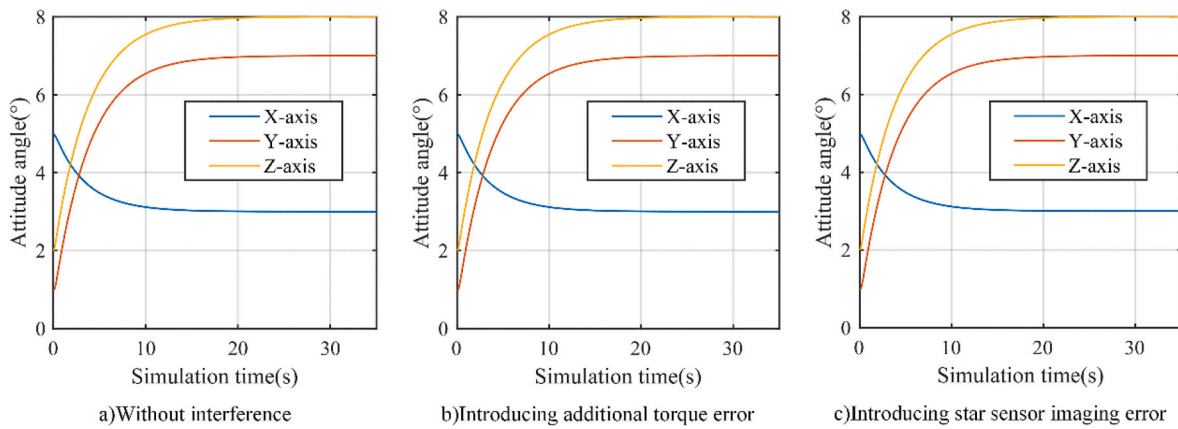
Fig. 12. Attitude angle change curve of maneuver condition #3.

Table 7
Statistics of rise time.

Maneuver condition	Without any interference	Introducing additional torque error	Introducing star sensor imaging error
#1	8.3921s (X-axis)	8.3922 s (X-axis)	8.3920 s (X-axis)
	8.2990 s (Y-axis)	8.2991 s (Y-axis)	8.2990 s (Y-axis)
	8.5124 s (Z-axis)	8.5124 s (Z-axis)	8.5125 s (Z-axis)
#2	8.1330 s (X-axis)	8.1331 s (X-axis)	8.1331 s (X-axis)
	7.8890 s (Y-axis)	7.8891 s (Y-axis)	7.8890 s (Y-axis)
	8.3855 s (Z-axis)	8.3855 s (Z-axis)	8.3854 s (Z-axis)
#3	7.5710 s (X-axis)	7.5709 s (X-axis)	7.5710 s (X-axis)
	8,3770 s (Y-axis)	8,3770 s (Y-axis)	8,3769 s (Y-axis)
	8.4135 s (Z-axis)	8.4134 s (Z-axis)	8.4134 s (Z-axis)

analysis of the influence of various disturbances on control system is also the focus of aerospace research field. Since most satellites use flywheels or control torque gyroscopes to adjust attitudes, and vibration isolation technology can not completely suppress or isolate micro vibrations, the method proposed in this paper has a relatively broad engineering application prospect. In the process of satellite design, this method can be used to simulate and analyze attitude control system accuracy. If the results cannot meet the engineering requirements, satellite's structure or control algorithm can be optimized based on time domain and frequency domain simulation result data, so as to minimize the impact of flywheel micro-vibration on attitude determination accuracy.

5. Conclusions

This paper proposes an effective modeling method that can introduce control torque error and star sensor imaging error caused by flywheel micro-vibration in typical satellite attitude control closed loop, and fully considers their influences on the accuracy of ACS by analyzing the mechanism of micro-vibration effect of the satellite principal prototype. It can be concluded that if the optical components in the star sensor are disturbed by excitation frequency close to structural modal frequency, misalignment might be caused, leading to imaging errors and the decrease of attitude determination accuracy at $0.4''$ level. Although the additional torque will also introduce jitter to the satellite principal prototype, its amplitude is so small that little impact is brought up on ACS. The results show that the micro vibration of flywheel may cause sub-second order jitter in the ACS. It is not enough to analyze the influence of micro vibration on LOS of optical payload, the errors of star sensor caused by micro vibration should also be introduced into the full-closed-loop simulation model. Furthermore, the two errors of micro-vibration introduced to ACS in this work must be considered for the development of spacecraft with $0.1''$ pointing accuracy.

Declaration of competing interest

The authors declare that they have no known competing financial interests or personal relationships that could have appeared to influence the work reported in this paper.

Acknowledgements

References

[1] L. Li, L. Yuan, L. Wang, et al., Recent advances in precision measurement & pointing control of spacecraft, Chin. J. Aeronaut. 34 (10) (2021) 191–209.
[2] D. Sakai, Y. Yoshimura, T. Hanada, et al., Contactless attitude control of an uncooperative satellite by laser ablation, Acta Astronaut. 196 (2022) 275–281.
[3] L. Li, L. Wang, L. Yuan, et al., Micro-vibration suppression methods and key technologies for high-precision space optical instruments, Acta Astronaut. 180 (4) (2020) 417–428.
[4] M. Plate, B. O'Sullivan, P. Ferruit, et al., The European optical contribution to the James Webb space telescope, Adv. Opt. Technol. 7 (6) (2018) 353–364.
[5] T. Obara, H. Matsumoto, K. Koga, Space environment measurements by JAXA satellites and ISS/JEM, Acta Astronaut. 71 (2012) 1–10.
[6] V. Amberg, C. Dechoz, L. Bernard, et al., In-flight attitude perturbations estimation: application to PLEIADES-HR satellites, Proc. SPIE 8866 (2013), 886612.
[7] F. Hu, X. Gao, G. Li, et al., Dem extraction from WORLDVIEW-3 stereo-images and accuracy evaluation, Int. Arch. Photogram. Rem. Sens. Spatial Inf. Sci. (2016) 12–19. Prague, Czech Republic.
[8] L. Yuan, M.M. Wang, Y.P. Wu, et al., Review on development of space starlight measurement technology, Acta Aeronautica Astronautica Sinica 41 (8) (2020) 7–18 +2 [Chinese].
[9] E. Turan, S. Speretta, E. Gill, Autonomous navigation for deep space small satellites: Scientific and technological advances, Acta Astronaut. 193 (2022) 56–74.
[10] L. Li, L. Yuan, L. Wang, et al., Image motion and experimental study of a 0.1″ space pointing measuring instrument for micro-vibration conditions, Chin. J. Aeronaut. 36 (2) (2023), https://doi.org/10.1016/j.cja.2022.02.003, 1991-200.
[11] L. Yang, Y. Wang, L. Wei, A novel identification method for micro-vibration analysis of reaction wheel assembly, Acta Astronaut. 196 (2022) 94–106.
[12] L. Li, Flywheel Micro-vibration Mechanism and Suppression Integrated Study for High Resolution Optical Satellite [dissertation], Changchun: University of Chinese Academy Sciences, 2018 [Chinese].
[13] Y. Zheng, Z. Zhou, H. Huang, A multi-frequency MIMO control method for the 6DOF micro-vibration exciting system, Acta Astronaut. 170 (2020) 552–569.
[14] L. Li, Li Tan, L. Kong, et al., The influence of flywheel micro-vibration on space camera and vibration sup-pression, Mech. Syst. Signal Process. 100 (2018) 360–370.
[15] D.W. Miller, O.L. Weck, G.E. Mosier, Framework for multidisciplinary integrated modeling and analysis of space telescopes, SPIE Proceedings, SPIE Workshop on Integrated Modeling of Telescopes 4757 (2002) 1–18. Lund, Sweden.
[16] M. Li, Y. Zhang, Y. Wang, et al., The pointing and vibration isolation integrated control method for optical payload, J. Sound Vib. 438 (2019) 441–456.
[17] D.M. LoBosco, C. Blaurock, S. Chung, et al., Integrated modeling of optical performance for the Terrestrial Planet Finder structurally connected

interferometer, SPIE Proceedings, Astronomical Telescopes & Instrumentation. USA 5497 (2004) 278–289.

[18] D.L. Aronstein, J.S. Smith, T.P. Zielinski, et al., Wavefront-error Performance Characterization for the James Webb Space Telescope (JWST) Integrated Science Instrument Module (ISIM) Science Instruments. SPIE Proceedings, SPIE Astronomical Telescopes & Instrumentation, Edinburgh, United Kingdom, 2016, 990409.

[19] F. Angeletti, P. Gasbarri, M. Sabatini, Optimal design and robust analysis of a net of active devices for micro-vibration control of an on-orbit large space antenna, Acta Astronaut. 164 (2019) 241–253.

[20] Z. Feng, Y. Cui, X. Yang, et al., Micro-vibration issues in integrated design of high resolution optical remote sensing satellites, Proceedings in Physics, 3rd International Symposium of Space Optical Instruments and Applications 192 (2017) 459–469. Springer, Cham.

[21] Y. Yu, X. Gong, L. Zhang, et al., Full-closed-loop time-domain integrated modeling method of optical satellite flywheel micro-vibration, Appl. Sci. 11 (3) (2021) 1328.

[22] X. Gong, L. Li, Y. Yu, et al., Error analysis and calibration of micro-vibration test platform developed for advanced pointing instrument, Mech. Syst. Signal Process. 173 (2022), 109055.

[23] F. Angeletti, P. Iannelli, P. Gasbarri, et al., End-to-end design of a robust attitude control and vibration suppression system for large space smart structures, Acta Astronaut. 187 (2021) 416–428.

[24] A. Rahimi, K.D. Kumar, H. Alighanbari, Fault detection and isolation of control moment gyros for satellite attitude control subsystem, Mech. Syst. Signal Process. 135 (2020), 106419.

[25] M. Christopher, H. Chris, The JWST integrated modeling environment, IEEE Aerospace Conference Proceedings (2004) 4041–4047, 2004.

[26] D. Ge, Y. Zou, Structure-control-optics integrated modeling and micro-vibration analysis for high resolution satellite 30 (6) (2013) 586–590.

[27] X. Guan, Integrated Design of Vibration Isolation and Attitude Control for High Resolution Remote Sensing Satellites. PhD Dissertation, Tsinghua University, 2012 [Chinese].

[28] X. Gong, L. Zhang, M. Xuan, Numerical modeling method for evaluation of image motion caused by flywheel disturbances, Acta Photonica Sin. 48 (5) (2019) 68–76 [Chinese].

[29] Q. Li, L. Liu, Y. Deng, et al., Twistor-based synchronous sliding mode control of spacecraft attitude and position, Chin. J. Aeronaut. 31 (5) (2018) 1153–1164.

[30] G.S. Aglietti, R.S. Langley, S.B. Gabriel, Model building and verification for active control of microvibrations with probabilistic assessment of the effects of uncertaities, Proc. Inst. Mech. Eng. PartC, Mech. Eng. Sci. 218 (4) (2004) 389–399.